Estimating the central charge from the Rényi entanglement entropy

A. Bazavov,[1,2,3] Y. Meurice,[1] S.-W. Tsai,[2] J. Unmuth-Yockey,[1,*] Li-Ping Yang,[4] and Jin Zhang[2]

[1]*Department of Physics and Astronomy, The University of Iowa, Iowa City, Iowa 52242, USA*
[2]*Department of Physics and Astronomy, University of California, Riverside, California 92521, USA*
[3]*Department of Computational Mathematics, Science and Engineering and Department of Physics and Astronomy, Michigan State University, East Lansing, Michigan 48824, USA*
[4]*Department of Physics,Chongqing University, Chongqing 401331, China*

(Received 5 April 2017; published 21 August 2017)

We calculate the von Neumann and Rényi bipartite entanglement entropy of the $O(2)$ model with a chemical potential on a $1+1$-dimensional Euclidean lattice with open and periodic boundary conditions. We show that the Calabrese-Cardy conformal field theory predictions for the leading logarithmic scaling of these entropies are consistent with a central charge $c=1$. This scaling survives the time-continuum limit and truncations of the microscopic degrees of freedom, modifications which allow us to connect the Lagrangian formulation to quantum Hamiltonians. At half-filling, the forms of the subleading corrections imposed by conformal field theory allow the determination of the central charge with an accuracy better than 2% for moderately sized lattices. We briefly discuss the possibility of estimating the central charge using quantum simulators.

DOI: 10.1103/PhysRevD.96.034514

I. INTRODUCTION

Conformal symmetry has been a major source of inspiration for theoretical physics during the last few decades [1,2]. In two dimensions, the conformal algebra is infinite dimensional and can be identified with the Virasoro algebra generating the reparametrization of the world sheet in string theory. This algebra admits central extensions labeled by the central charge, denoted c hereafter. Known unitary representations with $c=1-6/(m(m+1))$ and $m=3,\ldots,6$ describe the critical behavior of the two-dimensional Ising and 3-states Potts models and their tricritical versions [3–5]. For Z_n "clock" models with $n\geq 5$, the central charge and universality of the intermediate-temperature phase have been investigated numerically [6].

In three dimensions, the conformal bootstrap defines a boundary of the region of anomalous dimensions. On this boundary, there is a cusp, and there is a possibility that this cusp corresponds to the Ising universality class. This possibility has triggered very interesting new developments [7–9]. In four dimensions, the idea that electroweak symmetry breaking could result from new strong interactions at a multi-TeV scale with an approximate conformal symmetry [10–15] protecting a light Higgs-Brout-Englert boson has motivated numerous lattice studies [16–18].

QCD-like systems with various numbers of fundamental fermions and also fermions in different representations are being explored on the lattice (the latest results for various models are presented, for instance, in Refs. [19–23]). Based on the Banks-Zaks argument, systems with a large number of fermion flavors, N_f, feature a conformal phase [24]. However, precisely at what value of N_f, this happens for a particular gauge group, and fermion representation remains a subject of controversy. For the $SU(3)$ gauge group and fermions in the fundamental representation, some studies claim observing conformal behavior at $N_f=12$ (see Ref. [25] for instance), while others (e.g., Ref. [26]) argue that $N_f=12$ is not conformal.

To probe the conformality, various lattice methods, designed and well tested for QCD, have been employed. The major obstacle, however, is that large-N_f theories are very different from QCD. While in QCD the running of the coupling is fast enough so that one can probe both the ultraviolet perturbative and the infrared confining phenomena, as manifested, for instance, in one of the basic and extensively studied quantities, the static quark-antiquark potential, large-N_f theories require fine lattices and large volumes to disentangle the physics from the lattice cutoff effects. This makes identifying conformal theories from the massless extrapolations of massive lattice simulations a nontrivial task [25–30].

In the given examples, conformal symmetry is explicitly broken by the lattice regularization and only reemerges in a suitable continuum limit and infinite volume limit. Given the predictive power of conformal symmetries, it is important to identify the restoration of these symmetries in practical calculations at finite volumes. The entanglement entropy may offer a promising direction in understanding the conformal behavior of systems with finite-size scaling and could be a more sensitive tool, especially for small-size systems. How the entanglement entropy of a subsystem scales with its spatial volume provides useful information about the symmetries present and the conformality of the phases of a model [31]. This is very well understood in two (one space and one

*judah-unmuth-yockey@uiowa.edu

Euclidean time) dimensions where Calabrese and Cardy (CC) [32] have shown that various entanglement entropies scale like the logarithm of the size of the subsystem with coefficients proportional to the central charge.

Calculations of the entanglement entropy in lattice gauge theory with Monte Carlo methods have so far been performed in pure gauge theory [33–35] and two-dimensional critical spin systems [36]. Those calculations use the "replica trick" where n sheeted Riemannian surfaces are glued together over an interval but may require extra developments for theories with fermions. The entanglement spectrum for lower-order Rényi entanglement entropies has been analyzed for fermion systems in three dimensions using determinantal Monte Carlo methods, with universal behavior found that could potentially be observed in cold-atom experiments [37–39]. In the long run, finite-size scaling of the entanglement entropy may provide a cleaner way to study conformal systems than just increasing lattice volumes and decreasing lattice spacings in the hope of suppressing lattice artifacts.

In the following, we use renormalization group based methods [40–44] to calculate the von Neumann and second-order Rényi entanglement entropy of the classical $O(2)$ nonlinear sigma model with a chemical potential in $1+1$ dimensions on a space-time lattice. This model is often used as an effective theory for the Bose-Hubbard model [45] and is good as a toy model for gauge theories in higher dimensions. The model has vortex solutions, no long range order, and demonstrates a confinement-deconfinement transition of vortex-antivortex pairs. This model [46] has a superfluid (SF) phase where we expect to observe the CC scaling and multiple Mott insulator phase lobes lacking the CC scaling.

By using rectangular lattices of increasing spatial size and very large (Euclidean) temporal sizes, we probe the zero temperature entanglement entropy. We focus on half-integer charge density where the entropies considered are extremal. We then take the time-continuum limit and truncate the microscopic degrees of freedom in such a way that we obtain a Hamiltonian that can be quantum simulated [46,47]. These modifications should not affect the universal parts of the scaling. Our goal is to demonstrate that the constraints imposed by conformal symmetry on the finite-size scaling, as well as conjectures [48–50] explaining oscillations in the scaling, allow us to identify conformal behavior for modest lattice sizes.

The motivation for relating this model to a model that can be quantum simulated on optical lattices with cold atoms is prompted in current challenges with classical computation. It would be valuable to not only have efficient calculational tools for understanding conformal behavior for more complex, higher-dimensional systems but also to completely overcome the difficulty with large volume, small lattice spacing calculations entirely. This can be done by using quantum simulation, which can already reach volumes in $3+1$ dimensions on the same order as classical computation, and larger volumes are expected. This idea is pursued in more detail in Ref. [51].

Manipulations of small one-dimensional systems of cold atoms trapped in optical lattices have allowed experimental measurements of the second-order Rényi entanglement entropy [52] using a beam splitter method proposed in Ref. [53]. These measurements have been performed for small chains of four atoms. A more recent experiment on thermalization [54] involves six atoms. It is expected that in the near future manipulations of chains with 12 or more atoms will be possible [55].

The paper is organized as follows. In Sec. II, we review the Rényi entropy and the corresponding conventions used in this paper. We also discuss the currently understood asymptotic scaling in the Rényi entropy as a function of system size. In Sec. III, we introduce the $O(2)$ nonlinear sigma model on a lattice and the tensor formulation of the model. We give explicit tensor elements and discuss the isotropic and anisotropic coupling limits used in this paper as well as some results obtained in those limits. In Sec. IV, we give results for fits to Rényi entanglement entropy data. We consider the scaling of the entanglement entropy as a function of system size. We also go into detail about the methodology used in our fits and make comparisons with theoretical predictions. In Sec. V, we discuss the possibility of quantum simulating the $O(2)$ nonlinear sigma model and a possible quantum Hamiltonian that could be used for simulation. We also consider finite-temperature effects on the entanglement entropy. Finally, in Sec. VI, we give concluding remarks about in what possible directions work could proceed and other possible implications of this work.

II. RÉNYI ENTANGLEMENT ENTROPY

For the calculation of the entanglement entropy, we will restrict ourselves to $1+1$-dimensional space-time, or one space and one Euclidean time dimension, where the one-dimensional space has an even number of sites. For all results in this work, the system was divided into two identical parts, each one half the size of the entire spatial dimension, N_s (justification for this can be found in the supplemental material of Ref. [51]). Calculations of the entanglement entropy with other partitions of the system were exploratory and used as checks. Tracing over one of the halves, we obtain the reduced density matrix $\hat{\rho}_A$ for the other half (denoted A),

$$\hat{\rho}_A = \mathrm{Tr}_{\mathrm{env}}[\hat{\rho}], \tag{1}$$

where the trace is over the "environment" leaving only the subsystem defined as A. The nth-order Rényi entropy is defined as

$$S_n(A) \equiv \frac{1}{1-n}\ln(\mathrm{Tr}[\hat{\rho}_A^n]). \tag{2}$$

The limit $n \to 1^+$ is the von Neumann entanglement entropy, or the first-order Rényi entropy. S_2 is the second-order Rényi entropy and was measured in recent cold atom experiments [52]. An important goal for future work is to estimate the central charge, c, from empirical data. Using the transformation properties of the energy-momentum tensor and the Ward identities from conformal field theory (CFT), CC established that, to leading order, the Rényi entropy scales linearly with the logarithm of the spatial volume. The constant of proportionality is the central charge multiplied by a rational that depends on the order of the Rényi entanglement entropy and the boundary conditions:

$$S_n(N_s) = \begin{cases} K_n + \frac{c(n+1)}{6n}\ln(N_s) & \text{for PBC} \\ K_n' + \frac{c(n+1)}{12n}\ln(N_s) & \text{for OBC.} \end{cases} \tag{3}$$

The intercept is nonuniversal and different in the four situations considered here.

The calculation of S_n can be performed [56] using blocking (coarse-graining) methods [40–43]. In this work, we used the density matrix renormalization group (DMRG) with matrix product states (MPS) as well as exact blocking formulas [40–42,46] with the tensor renormalization group method (TRG), and the only approximation in these methods consists of truncating the number of states (called D_{bond}). The errors associated with this truncation will be discussed later.

III. $O(2)$ MODEL

In the following, we consider the classical $O(2)$ model on a $N_s \times N_\tau$ rectangular lattice with sites labeled (x,t). This is a generalization of the Ising model where the local spin is allowed to take values on a circle, making an angle θ with respect to some direction of reference. This angle can be interpreted as the phase of a complex field, and the model has an exact charge conjugation symmetry, $\theta \to -\theta$, interchanging particles and antiparticles. This symmetry can be broken by adding a chemical potential μ to the angle gradient [57]. The partition function reads

$$Z = \frac{1}{2\pi}\int \prod_{(x,t)} d\theta_{(x,t)} \mathrm{e}^{-S} \tag{4}$$

with

$$\begin{aligned} S = &-\beta_\tau \sum_{(x,t)} \cos(\theta_{(x,t+1)} - \theta_{(x,t)} - i\mu) \\ &- \beta_s \sum_{(x,t)} \cos(\theta_{(x+1,t)} - \theta_{(x,t)}). \end{aligned} \tag{5}$$

We use periodic boundary conditions (PBC) or open boundary conditions (OBC) in space and always PBC in time. In the following, we define the charge density as

$$\lambda \equiv \frac{1}{(N_s \times N_\tau)} \frac{\partial \ln(Z)}{\partial \mu}. \tag{6}$$

We will start with the situation where the relativistic interchangeability between space and time is present ($\beta_s = \beta_\tau \equiv \beta$), as is typical in lattice gauge theory simulations. Later, we will take the time-continuum limit and switch to the Hamiltonian formulation.

For numerical purposes, and in order to connect the Hamiltonian formulation to quantum simulators, it is convenient to introduce discrete degrees of freedom on the links (bonds) of the lattice. Using Fourier expansions [40,58,59], one can show [46,56] that the partition function can be expressed in terms of a transfer matrix $Z = \mathrm{Tr}[\mathbb{T}^{N_\tau}]$ where the matrix elements of $\mathbb{T}$ have the explicit form

$$\begin{aligned} \mathbb{T}_{(n_1,n_2,\ldots,n_{N_s})(n_1',n_2',\ldots,n_{N_s}')} = &\sum_{\tilde{n}_1\tilde{n}_2\ldots\tilde{n}_{N_s}} T^{(1,t)}_{\tilde{n}_{N_s}\tilde{n}_1 n_1 n_1'} T^{(2,t)}_{\tilde{n}_1\tilde{n}_2 n_2 n_2'} \cdots \\ &\times T^{(N_s,t)}_{\tilde{n}_{N_s-1}\tilde{n}_{N_s} n_{N_s} n_{N_s}'}, \end{aligned} \tag{7}$$

with

$$\begin{aligned} T^{(x,t)}_{\tilde{n}_{x-1}\tilde{n}_x n_t n_t'} = &\sqrt{I_{n_t}(\beta_\tau) I_{n_t'}(\beta_s) \exp(\mu(n_t + n_t'))} \\ &\times \sqrt{I_{\tilde{n}_{x-1}}(\beta_s) I_{\tilde{n}_x}(\beta_\tau)}\, \delta_{\tilde{n}_{x-1}+n_t, \tilde{n}_x + n_t'}. \end{aligned} \tag{8}$$

In Eq. (8), the first two indices are associated with the links in the spatial direction, while the last two indices are associated with the links in the temporal direction. When N_s is a power of 2, the traces in the spatial directions in Eq. (7) can be performed recursively and combined with a truncation of the number of states kept in the time direction [46,56]. The accuracy of this tensor renormalization group method has been tested against sampling methods [56].

We can interpret $\mathbb{T}^{N_\tau}$ as a density matrix $\hat{\rho}$ if we normalize by the trace of the matrix. It is important to understand that the classical spin model described above can be taken in a limiting form as a quantum model in one spatial dimension. In the following, we always take $N_\tau \gg N_s$ and extrapolate to infinite N_τ. This corresponds to the zero-temperature limit in the quantum terminology. Finite-temperature effects will be discussed in Sec. V and were considered in Ref. [56].

The SF phase is characterized by a response of the charge density, λ, to a change in the chemical potential. This is illustrated in Refs. [46,59]. In contrast, in the Mott phases, the charge density keeps a fixed integer value as we increase μ. This lack of response is somewhat puzzling in the functional integral formulation and is often called the "Silver blaze" phenomenon [60] in the context of finite-temperature QCD. Another characterization of the two phases is by the scaling of the Rényi entropy as a function of the volume of space.

In the following, we focus on two cases for two different relationships between the spatial and temporal couplings. We consider $\beta = 0.1$, $\mu \simeq 3$ (case 1), and $\beta = 2$, $\mu = 0$ (case 2). Both of these situations are considered in the limits of isotropic coupling ($\beta_s = \beta_\tau$) and anisotropic coupling ($\beta_s\beta_\tau = \text{const.}$. with $\beta_\tau \to \infty$ and $a \to 0$, where a is the temporal lattice spacing). In case 1, the SF transition is driven by an increase in the chemical potential at fixed β. This is the transition driven by fluctuations in density. For case 2, the transition is driven by the presence of vortices and is the Berezinskii-Kosterlitz-Thouless transition.

A. Isotropic coupling

In this section, we consider the case where the coupling in space and time are the same. This is a classical statistical two-dimensional spin system. Using TRG, we can block a (Euclidean) time slice of the lattice and consider it a transfer matrix. From it, we can calculate a "zero-temperature" density matrix by taking $N_\tau \gg N_s$ (typically $N_\tau \approx 2^{20}N_s$ in practice, although even larger sizes may be used). Then, from the density matrix, one can make the reduced density matrix and calculate the Rényi entropy of the desired order.

The values of S_1 and S_2 are shown in Fig. 1 for $N_s = 4$, 8, 16, and 32, for PBC and OBC. These results are compared with the leading CFT prediction of Eq. (3) by just fitting the intercept with the CFT slope fixed. For isotropic calculations, the TRG calculations kept up to 250 states. The figure shows that the discrepancies are rather small and most visible for S_2 with OBC for case 1. In case 2, the discrepancies are slightly more pronounced. In all cases, the discrepancies are due to subleading corrections not taken into account in the fits, rather than the small numerical errors.

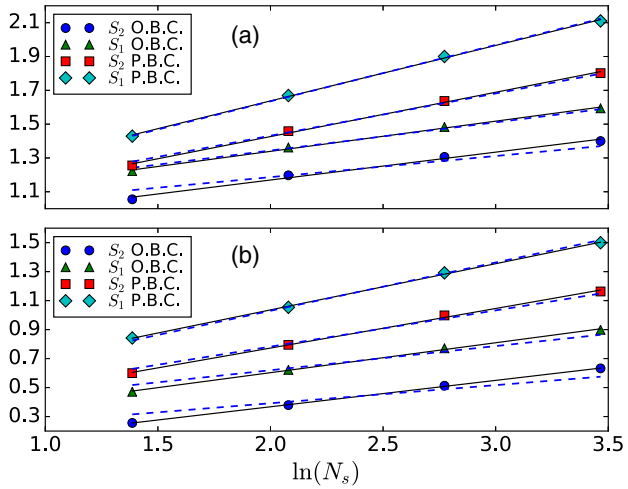

FIG. 1. (a) The second-order (S_2) and first-order Rényi (S_1) entropies for case 1, $\mu = 2.99$ and $\beta_s = \beta_\tau = 0.1$, both PBC and OBC. The solid, black lines are linear fits to the data, and the dashed, blue (online) lines are fits of the intercept with the CFT slopes. (b) Same quantities for case 2, $\mu = 0$ and $\beta_s = \beta_\tau = 2$.

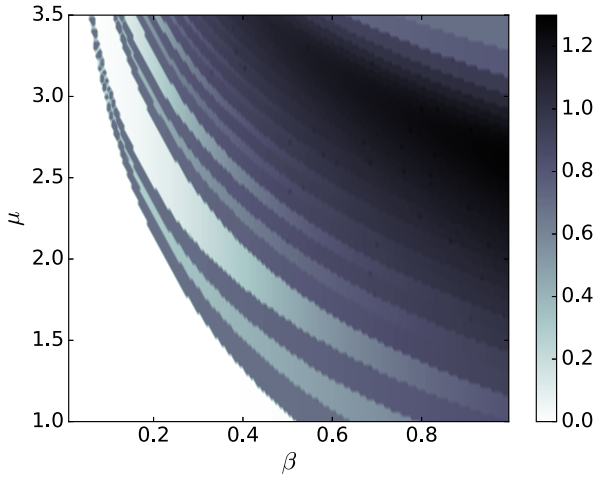

FIG. 2. Second-order Rényi entropy in the β-μ plane for $N_s = 4$ showing the various lobes of charge densities. $\lambda = 0$, 1, and 2 are the prominent bright regions stemming from the $\beta = 0$ axis.

Figure 2 gives the values of S_2 for $N_s = 4$ across a region of the β-μ plane. This figure shows lobes corresponding to a fixed charge density. The largest and most prominent is the $\lambda = 0$ lobe, followed by a much thinner $\lambda = 1$ lobe above. The lobes continue as long as the truncation on the number of states used in the TRG calculation can support the charge density. Figure 2 also shows three plateaus in the SF regions between each Mott lobe. These plateaus were investigated and related to the charge density in the isotropic limit in [56]. In the next section, we consider the time-continuum limit of the classical $O(2)$ model and how the phase diagrams transform through taking that limit.

B. Anisotropic coupling

We now proceed to take the time-continuum limit. This can be achieved by taking β_τ very large while keeping constant the product $\beta_s\beta_\tau$ and keeping $\mu\beta_\tau$ tuned to the desired charge density. For case 1, the limit of the chemical potential must be done carefully in order to maintain a fixed charge density corresponding to half-filling. For small volumes, half-filling takes place around $\mu\beta_\tau = 0.5$ as $\beta_\tau \to \infty$, but not all the data collected for larger volumes were necessarily done at that parameter specification, and instead the parameters were tuned to maintain half-filling. The time-continuum limit in the tensor formulation defines [46] a rotor Hamiltonian [61,62],

$$\hat{H} = \frac{U}{2}\sum_x \hat{L}_x^2 - \tilde{\mu}\sum_x \hat{L}_x - 2J\sum_{\langle xy\rangle}\cos(\hat{\theta}_x - \hat{\theta}_y), \quad (9)$$

with $[\hat{L}_x, e^{i\hat{\theta}_y}] = \delta_{xy}e^{i\hat{\theta}_y}$. It is possible to truncate to finite integer spin and approximate these commutation relations [46]. The normalization has been chosen in such a way that

the coupling constants in the Bose-Hubbard model used in Ref. [52] and here in the $O(2)$ model are the same: $\beta_s\beta_\tau \equiv 2J/U$ and $\mu\beta_\tau \equiv \tilde{\mu}/U$.

In the following, we primarily use the spin-1 approximation, which can also be implemented in the original isotropic formulation by setting the tensor elements in Eq. (8) to zero for space and time tensor indices strictly larger than 1 in absolute value (so only three states remain). The Hamiltonian is then a spin-1 XY model with a chemical potential and an ion anisotropy. In addition, for large enough chemical potential, the $n = -1$ component decouples, and we are approximately left with a spin-1/2 XY model. Furthermore, for $\tilde{\mu} = U/2 \gg J$, there is an approximate connection with the Bose-Hubbard model

$$H = \frac{U}{2}\sum_x n_x(n_x - 1) - J\sum_x (a_x^\dagger a_{x+1} + \text{H.c.}). \qquad (10)$$

The Hamiltonian in Eq. (9) is never explicitly used in the blocking procedure with TRG. In practice, the TRG tensors used are the same; however, the coupling constants that appear in the local tensor's definition are tuned to reflect the scenario under consideration. Again, using the TRG the same way, one calculates the Rényi entropy for an approximately zero-temperature situation. The only minor change is that, due to the increased coupling in the time direction, N_τ needs to be adjusted to compensate the smaller lattice spacing. This means increasing N_τ even more, a facile task while using a blocking method. We show slices of the Rényi entropy in the region of case 1 for $N_s = 4$ and 8, OBC, in Fig. 3. A more extensive plot of S_2 for the $O(2)$ model in the time-continuum limit can be found in Ref. [51] for a large range of couplings along with a comparison to the Bose-Hubbard model.

In order to check the TRG calculations of S_n in the time-continuum limit [Eq. (9)], we have used DMRG [43], which has been used to calculate the ground state entanglement entropy and Rényi entropy for similar Hamiltonians [63–65]. Calculations with MPS optimization [44] have been performed using the ITensor C++ library [66]. We run enough sweeps for the entropy to converge to at least 10^{-8}, and a large number of states, up to 1500, was kept so that the truncation error is less than 10^{-10}. The comparison of the results with the two methods showed excellent agreement at small volume (typically nine digits for $N_s = 4$), but the discrepancies increased with the volume (typically three digits agreement for $N_s = 32$). We believe that the DMRG results are more accurate because, first, it can keep many more states than the TRG by using sparse linear algebra libraries. Second, the truncations are made step by step to try to maximize the entanglement entropy. Finally, DMRG uses an environment sweep method which optimizes the ground state wave function iteratively. For these reasons, we have used the DMRG results for the fits that follow.

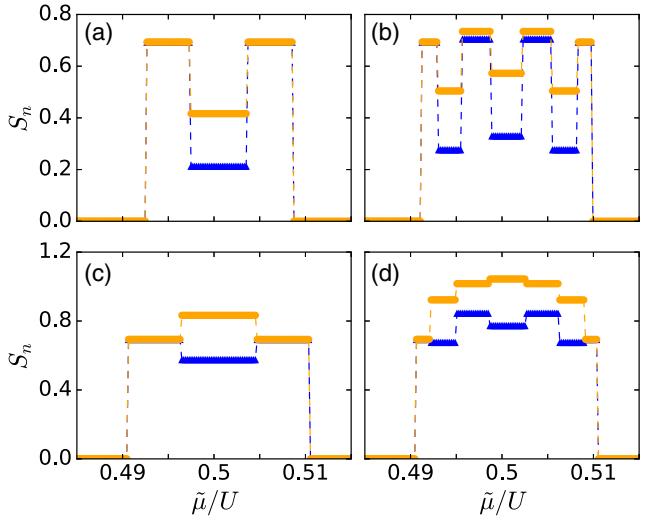

FIG. 3. The first-order (orange online) and second-order (blue online) Rényi entropy as a function of $\tilde{\mu}/U$ in the region around case 1. (a), (b) Entropies for $N_s = 4$ and $N_s = 8$, respectively, with OBC. (c), (d) Entropies for $N_s = 4$ and $N_s = 8$, respectively, with PBC. The second Rényi entropy maintains a local minimum around $\tilde{\mu}/U = 0.5$ for all cases; however, the PBC data for the first Rényi entropy have a maximum. For these data, $\beta_\tau = 500$ and $D_{\text{bond}} = 101$.

IV. FITS TO S_n

In this section, we give some results for fits to the isotropic and anisotropic data, as well as for fits to the DMRG data. The primary deviations from the leading-order linear behavior of the Rényi entropy come from finite volume effects and parity oscillations. These deviations were found most prominently in OBC data and the second-order Rényi entropy. Oscillations were found between sizes N_s mod $4 = 0$ and N_s mod $4 = 2$, although in case 1 S_1 with PBC had none, as well as S_1 in case 2. Corrections to the leading-order CFT behavior to account for these oscillations have been conjectured [48–50], and we check their validity for the anisotropic $O(2)$ model. In addition, nonoscillatory finite-volume corrections have been derived [67], and in the following, we attempt to take all these corrections into account in order to fit the data as well as possible.

Initially, all the data were fit to the leading-order CFT prediction [Eq. (3)], with the slope and intercept as the two free parameters. This was done for spatial volumes which matched the TRG blocking volumes, e.g., $N_s = 2^\ell$, and since these sizes are multiples of 4, no oscillations were present. These fits were done for both the DMRG and TRG data in both the isotropic and anisotropic limits. The results for the slope fits are reported in Table I for all cases considered.

For the two cases considered here, we tried various fits that attempted to incorporate subleading corrections. We attempted fits with four or five free parameters. These included corrections $\propto 1/N_s$, $1/N_s^2$, $1/\ln(N_s)$ and

TABLE I. Slopes of the Rényi entropies using the leading-order linear fit. The fits were done using the same volumes used in the TRG calculations: $N_s = 2^\ell$. For data at these volumes, oscillations do not appear; oscillations occur between volumes: N_s mod $4 = 0$ and N_s mod $4 = 2$.

Case 1	Isotropic	Anisotropic	DMRG	$c = 1$ CFT
S_1 PBC	0.319	0.311	0.327	$0.\bar{3}$
S_2 PBC	0.273	0.265	0.267	0.25
S_1 OBC	0.207	0.208	0.195	$0.1\bar{6}$
S_2 OBC	0.182	0.152	0.168	0.125
Case 2	Isotropic	Anisotropic	DMRG	$c = 1$ CFT
S_1 PBC	0.328	0.296	0.329	$0.\bar{3}$
S_2 PBC	0.262	0.229	0.250	0.25
S_1 OBC	0.179	0.152	0.159	$0.1\bar{6}$
S_2 OBC	0.165	0.148	0.140	0.125

$1/\ln^2(N_s)$. To judge the quality of the fits, we compared the average relative error between fits,

$$(\text{relative error})^2 = \frac{1}{N}\sum_{i=1}^{N}\left(\frac{y_i - f(x_i)}{y_i}\right)^2, \qquad (11)$$

with y_i the dependent data and $f(x_i)$ the fitting function evaluated at the independent data. This measure is convenient since the error is dimensionless; in addition, a χ^2 measure of error would depend upon the unknown DMRG error bars, and fitting with uncertainties in arbitrary units gives a relatively useless estimate of the fit quality. The relative errors associated with the fits were never greater than 10^{-3} and never less than 10^{-7}. For systems with subsystems of size l, we considered a fit of the form

$$S_n(N_s, l) = A_n \ln\left\{N_s \sin\left[\frac{\pi l}{N_s}\right]\right\} + B + \frac{C}{N_s^{p_n}}\cos(\pi l)\left|\sin\left[\frac{\pi l}{N_s}\right]\right|^{-p_n} + f_n(N_s, l) \qquad (12)$$

with f_n a function to take into account additional corrections, and A_n, B, C, and p_n are fit parameters. However, we focused on data with $l = N_s/2$. We found the best fit results by excluding data with $l < N_s/2$ and $l > N_s/2$ for small N_s, and at larger N_s, we found fits preferred data near $l \approx N_s/2$, resulting in data which resembled a "fan with a handle" (see Ref. [51]).

For case 1, the best fits included corrections like $f \propto 1/N_s^2$ and $1/\ln^2(N_s)$. We found almost identical relative errors between corrections $1/N_s^2$ and $1/\ln^2(N_s)$. For case 2, the OBC data had the least error with corrections $\propto 1/N_s$, while the PBC data had the least error with corrections $\propto 1/N_s^2$. For the oscillating term, the various p_n are expected to follow special relations [49] (see below). For some fits, there were no oscillations present, and the fits drove p_n very large. In these cases, we replaced the $\pi N_s/2$ in the cosine by πN_s, so as to set it to unity by hand, and assumed a correction $\propto N_s^{-p_n}$. The fits were done by nonlinear least-squares minimization.

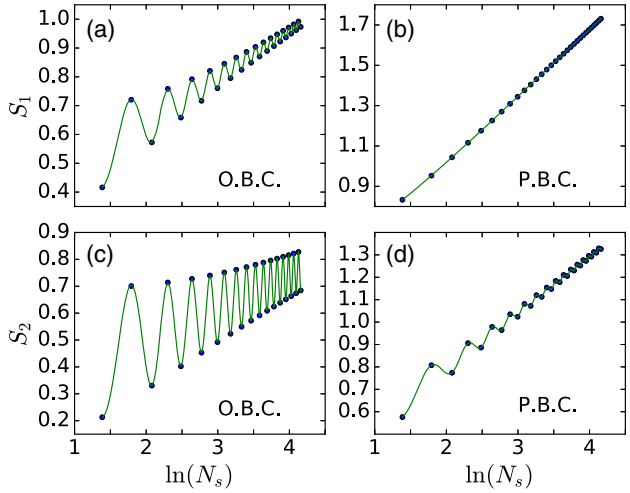

FIG. 4. The first-order and second-order Rényi entropy scaling with system size for $\beta_s\beta_\tau = 0.01$, $\mu\beta_\tau = 0.5$ in the time-continuum limit calculated using DMRG. (a), (b) The first-order Rényi entropy with OBC and PBC, respectively. (c), (d) The second-order Rényi entropy with OBC and PBC, respectively.

The results are shown in Fig. 4 for case 1. The values of the slopes, A_n, for both S_1 and S_2 are plotted in Fig. 5 with the slope value predicted from CFT surrounded by a band representing a 1% deviation from the CFT value. The values for A_n and p_n using all the data points up to $N_s = 64$ are shown in Table II. Notice the good agreement with the predicted relations [49] $p_1^{\text{OBC}} = 2p_2^{\text{OBC}}$, $p_1^{\text{PBC}} = 2p_2^{\text{PBC}}$,

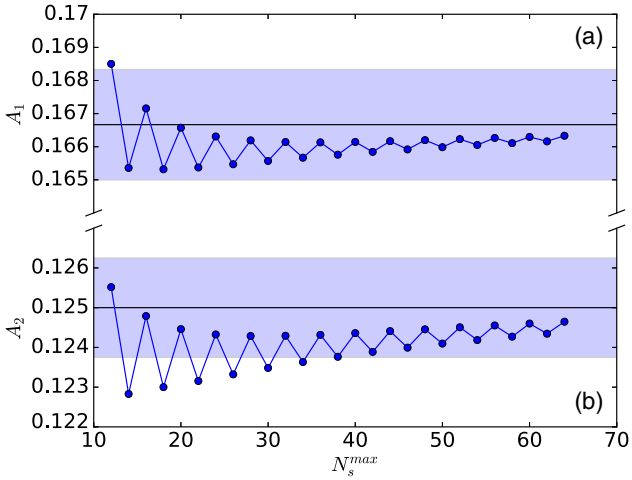

FIG. 5. The A_n for $\beta_s\beta_\tau = 0.01$, $\mu\beta_\tau = 0.5$ with OBC is plotted vs the maximal size of the lattice used to fit the data. The horizontal line is the CFT prediction with $c = 1$ with a region around representing a $\pm 1\%$ deviation. (a) The first-order Rényi entropy. (b) The second-order Rényi entropy.

TABLE II. Values for A_n and p_n for $\beta_s\beta_\tau = 0.01$, $\mu\beta_\tau = 0.5$, from the least-squares fits to the DMRG data up to $N_s = 64$ corresponding to Fig. 4.

S_n	p_n	A_n from fit	A_n with $c = 1$
S_1 PBC	2.315	0.3338	$0.\bar{3}$
S_2 PBC	0.981	0.2525	0.25
S_1 OBC	0.901	0.1663	$0.1\bar{6}$
S_2 OBC	0.443	0.1246	0.125

TABLE III. Values for A_n for $\beta_s\beta_\tau = 4$, $\mu\beta_\tau = 0$, from the least-squares fits to the DMRG data up to $N_s = 64$ corresponding to Fig. 6.

S_n	A_n from fit	A_n with $c = 1$
S_1 PBC	0.3337	$0.\bar{3}$
S_2 PBC	0.2500	0.25
S_1 OBC	0.1654	$0.1\bar{6}$
S_2 OBC	0.1278	0.125

and $p_n^{\mathrm{PBC}} = 2p_n^{\mathrm{OBC}}$. The fit results for case 2 are shown in Fig. 6. As can be seen, the oscillations are very small, if at all, as compared to case 1. Also, in contrast, case 2 did not yield the special relationships between the p_n exponents that did occur for case 1. The A_n values when fitting to all the data up to $N_s = 64$ are found in Table III. In both case 1 and case 2, the first-order Rényi (von Neumann) entropy with PBC possesses no oscillations, which is in agreement with what is known [48]. These results suggest that both of these different regions of the phase diagram are conformal and approximately $c = 1$. If either of these two regimes could be quantum simulated and experimentally realized, it may be possible to measure the central charge. We will briefly discuss the feasibility of this prospect in the next section.

V. PROSPECT FOR QUANTUM SIMULATIONS

To better understand the possibility of quantum simulating the $O(2)$ model, it is important to find a suitable condensed matter model to relate to. We considered a single species Bose-Hubbard quantum Hamiltonian [Eq. (10)] in a region of the phase diagram where the two models are essentially identical: $\tilde{\mu} \approx U/2 \gg J$, i.e., similar to case 1. While the hopping parameter is very small compared to the on-site repulsion, the chain is only *half-filled*, allowing the superfluid regime to be probed.

We considered the second-order Rényi entropy for the Bose-Hubbard model for $J/U = 0.005$ and $J/U = 0.1$ with OBC. We did runs using DMRG across various system sizes such that $4 \le N_s \le 64$ and subsystem sizes such that $1 \le l \le N_s - 1$. To illuminate the legitimacy of the comparison between the two models, we have plotted S_2 and A_2 for both the $O(2)$ model in the time-continuum limit for case 1 and the Bose-Hubbard model with $J/U = 0.005$ in Fig. 7. As one can see in Fig. 7, the BH model in this limit is almost identical to case 1 of the $O(2)$ model. Changing J/U to 0.1 increases the discrepancy, but the models continue to agree quantitatively well, especially for smaller volumes. The exploratory fits and trials can be found in Ref. [51]. A Bose-Hubbard model with small spatial volumes and $\mu = U/2 \gg J/U = 0.1$ appears as a potential candidate for quantum simulating the $O(2)$ model and experimentally measuring the central charge.

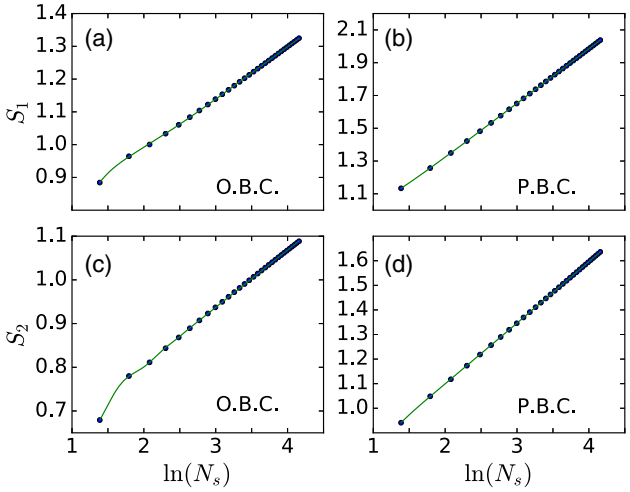

FIG. 6. The first-order and second-order Rényi entropy scaling with system size for $\beta_s\beta_\tau = 4$, $\mu\beta_\tau = 0$ in the time-continuum limit calculated using DMRG. (a), (b) The first-order Rényi entropy with OBC and PBC, respectively. (c), (d) The second-order Rényi entropy with OBC and PBC, respectively.

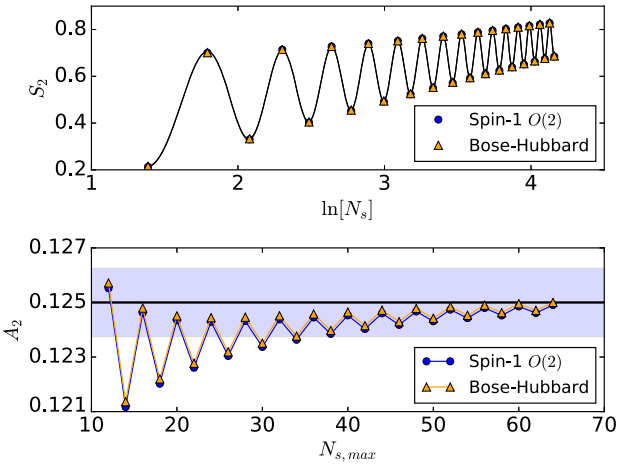

FIG. 7. A comparison between the Bose-Hubbard model and the $O(2)$ model at half-filling and $J/U = 0.005$ with OBC. (top) S_2 for the two models. The data lie almost on top of each other, and there are two solid black lines fitting the two data sets which are essentially indistinguishable. (bottom) The value of A_2 vs the maximum size of the lattice used to extract the value of A_2. The horizontal line represents the CFT prediction of $1/8$ with a band representing a $\pm 1\%$ deviation.

The possibility of measuring the central charge with cold atoms trapped in optical lattices was investigated in Ref. [51].

A. Finite-temperature effects

For quantum simulation, while most of the calculations were done at $T = 0$, finite-temperature effects should be considered. Here, we take k, the Boltzmann constant, equal to unity. While working on a two-dimensional Euclidean lattice, we must relate the temporal extent to the physical temperature. This is done through the relation

$$\frac{1}{T} = N_\tau a. \tag{13}$$

This relation can be derived with simple quantum statistical mechanics arguments. To take the time-continuum limit, we allowed $\beta_\tau \to \infty$ and $a \to 0$. This allowed us to set the scale with the quantity $U \equiv 1/\beta_\tau a$. With this definition, we have

$$\frac{1}{T} = \frac{N_\tau}{\beta_\tau U} = \frac{\beta_s N_\tau}{2J}. \tag{14}$$

This relates a number of important quantities, for instance, the spatial or temporal coupling on the Euclidean lattice to the physical temperature of a quantum Hamiltonian, as well as the number of temporal sites on the lattice. In addition, it relates the hopping parameter, J, and the on-site repulsion, U, to the physical temperature and lattice couplings.

To verify this relation between the classical picture of a two-dimensional lattice and its quantum counterpart in one less dimension, we again compared time-continuum TRG results with DMRG results for finite temperature. For TRG, we merely considered temporal lattice sizes which were not as great as before for the zero-temperature analysis and tuned the couplings for the time-continuum limit. The DMRG analysis used a thermal density matrix (as opposed to using the ground state) to compute the Rényi and von Neumann entanglement entropies [68–70]. In Fig. 8, one can see the agreement between the DMRG calculations and the TRG ones in the case of the $O(2)$ model. This figure also demonstrates the effect the thermal entropy has on the entanglement entropy as the temperature increases. The peaks and valleys of the entanglement entropy become smoothed out, and while the boundaries remain at approximately ln(2), the half-filling valley increases.

For systems at half-filling, i.e., the central peak (valley) like in Figs. 3 and 8, the CC scaling can be well fit to a functional form

$$S_n(N_s) = A_n \ln(N_s) + B + \frac{C}{N_s^{p_n}} \cos(\pi N_s/2) + EN_s + f(N_s), \tag{15}$$

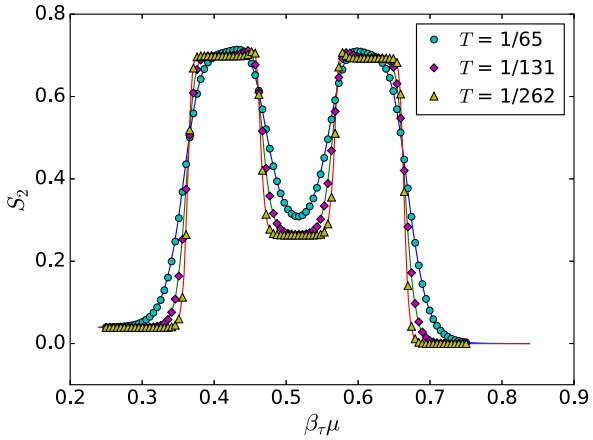

FIG. 8. The second-order Rényi entropy as a function of the chemical potential, $\tilde{\mu} = \beta_\tau \mu$, for $N_s = 4$ with $J/U = 0.1$. The solid lines are the DMRG data and the markers are the TRG data. We see the effects of a finite temperature on S_2 are to smooth out the peaks and valleys. As the temperature increases, the thermal entropy dominates the Rényi entropy. The temperature, T, was calculated here with $U = 1$ and $\beta_\tau = 500$, and $D_{\text{bond}} = 201$ for the TRG.

that is, adding a term linear in N_s takes into account the finite-temperature effects. For fits to a general subsystem size at fixed N_s, we find a term linear in l fits the data well,

$$S_n(N_s, l) = A_n \ln\left\{\frac{4(N_s+1)}{\pi} \sin\left[\frac{\pi(2l+1)}{2(N_s+1)}\right]\right\} + B + \frac{C}{N_s^{p_n}} \sin\left[\frac{\pi(2l+1)}{2}\right] \left| \sin\left[\frac{\pi(2l+1)}{2(N_s+1)}\right]\right|^{-p_n} + Dl + f_n(N_s, l). \tag{16}$$

This linear term can be used to subtract off finite-temperature effects [54]; however, we find additional corrections are necessary to maintain the original $T = 0$ fit parameters. Examples of fits done with these functional forms for various temperatures can be found in Ref. [51].

VI. CONCLUSION

We have argued that finite-size scaling of the entanglement entropy may provide a sensitive tool for identifying conformal behavior in a system. It may complement the techniques currently in use in the lattice gauge theory community for studying models in the context of physics beyond the Standard Model. Such models are harder to study on the lattice than QCD, because the running of the coupling is slow and the relevant physics may be easily masked by lattice artifacts (e.g., finite lattice spacing and finite volume).

We have calculated the Rényi entropy for the classical $O(2)$ model in the isotropic coupling limit, as well as in the anisotropic coupling limit with a quantum Hamiltonian. From fits to the Rényi entropy, we have estimated the

central charge. We found that this model can be mapped to a single-species Bose-Hubbard model in a particular region of the phase diagram and their Rényi entropies are quantitatively similar, allowing for the possibility of quantum simulating the $O(2)$ model and observing the CC scaling during simulation. In addition, we have considered finite-temperature effects on the Rényi entropy and found fitting functions which match the data for S_2 well, with scaling in N_s and in subsystem size. These additional fits involved including a term which is linear in either the subsystem size, l, or the system size, N_s.

It would be interesting to study the scaling of the Rényi entropy of the $O(3)$ nonlinear sigma model with finite chemical potential in $1+1$ dimensions. This model is known to have asymptotic scaling in the continuum limit leading to a nonzero mass gap, as well as meron (instanton) solutions that are related to vortices in the $O(2)$ nonlinear sigma model [71,72]. With the inclusion of a chemical potential coupled to the $O(2)$ subgroup it is, as of now, unclear what sort of transition takes place at finite density. The phase diagram in the time-continuum limit has a form similar [73] to the $O(2)$ model considered here and could be investigated in a similar fashion.

In addition, it would be interesting to study the effects of a weak gauge coupling to the $O(2)$ spins (as discussed in Refs. [47,74]). This would be scalar electrodynamics in a perturbative limit of weak gauge coupling. Monitoring the entanglement entropy as one takes the limit of zero gauge coupling would give information about the symmetries for the phases of scalar electrodynamics and the passage between the two models.

ACKNOWLEDGMENTS

We thank M. C. Banuls, I. Bloch, I. Cirac, M. Greiner, A. Kaufman, G. Ortiz, J. Osborn, H. Pichler, and P. Zoller for useful suggestions or comments as well as Philipp Preiss for input on experimental aspects of quantum simulating with cold atoms on optical lattices. This research was supported in part by the Department of Energy under Grants No. DE-SC0010114, and No. DE-FG02-91ER40664; the NSF under Grant No. DMR-1411345; and by the Army Research Office of the Department of Defense under Award No. W911NF-13-1-0119. L. -P. Yang was supported by Natural Science Foundation for young scientists of China (Grant No. 11304404) and Research Fund for the Central Universities (Grant No. CQDXWL-2012-Z005). Parts of the numerical calculations were done at the Argonne Leadership Computational Facilities. Y. M. thanks the Focus Group Physics with Effective Field Theories of the Institute for Advanced Study, Technische Universität München, and the workshop on "Emergent properties of space-time" at CERN for hospitality while part of this work was carried out and the Institute for Nuclear Theory for motivating this work during the workshop "Frontiers in Quantum Simulation with Cold Atoms".

[1] A. M. Polyakov, *Gauge Fields and Strings*, Contemporary Concepts in Physics (Taylor and Francis, London, 1987).
[2] P. Di Francesco, P. Mathieu, and D. Sénéchal, *Conformal Field Theory*, Graduate Texts in Contemporary Physics (Springer, New York, 1997).
[3] A. A. Belavin, A. M. Polyakov, and A. B. Zamolodchikov, Nucl. Phys. **B241**, 333 (1984).
[4] D. Friedan, Z. Qiu, and S. Shenker, Phys. Rev. Lett. **52**, 1575 (1984).
[5] V. S. Dotsenko, Nucl. Phys. **B235**, 54 (1984).
[6] P. Suranyi, Nucl. Phys. **B300**, 289 (1988).
[7] S. El-Showk, M. F. Paulos, D. Poland, S. Rychkov, D. Simmons-Duffin, and A. Vichi, Phys. Rev. D **86**, 025022 (2012).
[8] S. El-Showk, M. F. Paulos, D. Poland, S. Rychkov, D. Simmons-Duffin, and A. Vichi, J. Stat. Phys. **157**, 869 (2014).
[9] F. Kos, D. Poland, and D. Simmons-Duffin, J. High Energy Phys. 11 (2014) 109.
[10] T. Appelquist, J. Terning, and L. C. R. Wijewardhana, Phys. Rev. Lett. **77**, 1214 (1996).
[11] V. A. Miransky and K. Yamawaki, Phys. Rev. D **55**, 5051 (1997).
[12] R. S. Chivukula, Phys. Rev. D **55**, 5238 (1997).
[13] T. Appelquist and F. Sannino, Phys. Rev. D **59**, 067702 (1999).
[14] M. A. Luty and T. Okui, J. High Energy Phys. 09 (2006) 070.
[15] D. D. Dietrich, F. Sannino, and K. Tuominen, Phys. Rev. D **72**, 055001 (2005).
[16] T. DeGrand, Phil. Trans. R. Soc. A **369**, 2701 (2011).
[17] T. Blum *et al.*, arXiv:1310.6087.
[18] J. Kuti, *Proc. Sci.*, KMI2013 (2015) 002.
[19] T. DeGrand, Y. Liu, E. T. Neil, Y. Shamir, and B. Svetitsky, Phys. Rev. D **91**, 114502 (2015).
[20] R. C. Brower, A. Hasenfratz, C. Rebbi, E. Weinberg, and O. Witzel, Phys. Rev. D **93**, 075028 (2016).
[21] R. Arthur, V. Drach, M. Hansen, A. Hietanen, C. Pica, and F. Sannino, Phys. Rev. D **94**, 094507 (2016).
[22] T. Appelquist *et al.* (Lattice Strong Dynamics [LSD] Collaboration), Phys. Rev. D **93**, 114514 (2016).
[23] Z. Fodor, K. Holland, J. Kuti, S. Mondal, D. Nogradi, and C. H. Wong, Phys. Rev. D **94**, 014503 (2016).
[24] T. Banks and A. Zaks, Nucl. Phys. **B196**, 189 (1982).
[25] A. Cheng, A. Hasenfratz, Y. Liu, G. Petropoulos, and D. Schaich, J. High Energy Phys. 05 (2014) 137.

[26] Z. Fodor, K. Holland, J. Kuti, S. Mondal, D. Nogradi, and C. H. Wong, Phys. Rev. D **94**, 091501 (2016).
[27] A. Hasenfratz, Phys. Rev. Lett. **108**, 061601 (2012).
[28] Z. Fodor, K. Holland, J. Kuti, D. Nogradi, and C. Schroeder, Phys. Lett. B **703**, 348 (2011).
[29] Y. Aoki, T. Aoyama, M. Kurachi, T. Maskawa, K. I. Nagai, H. Ohki, A. Shibata, K. Yamawaki, and T. Yamazaki (LatKMI Collaboration), Phys. Rev. D **86**, 054506 (2012).
[30] Z. Gelzer, Y. Liu, and Y. Meurice, *Proc. Sci.*, LATTICE2014 (2014) 255.
[31] N. Schuch, M. M. Wolf, F. Verstraete, and J. I. Cirac, Phys. Rev. Lett. **100**, 030504 (2008).
[32] P. Calabrese and J. L. Cardy, J. Stat. Mech. (2004) P06002.
[33] A. Velytsky, Phys. Rev. D **77**, 085021 (2008).
[34] P. V. Buividovich and M. I. Polikarpov, Nucl. Phys. **B802**, 458 (2008).
[35] E. Itou, K. Nagata, Y. Nakagawa, A. Nakamura, and V. I. Zakharov, Prog. Theor. Exp. Phys. **2016**, 061B01 (2016).
[36] M. Caraglio and F. Gliozzi, J. High Energy Phys. 11 (2008) 076.
[37] W. J. Porter and J. E. Drut, Phys. Rev. B **94**, 165112 (2016).
[38] J. E. Drut and W. J. Porter, Phys. Rev. E **93**, 043301 (2016).
[39] J. E. Drut and W. J. Porter, J. Phys. A **50**, 145304 (2017).
[40] Y. Liu, Y. Meurice, M. P. Qin, J. Unmuth-Yockey, T. Xiang, Z. Y. Xie, J. F. Yu, and H. Zou, Phys. Rev. D **88**, 056005 (2013).
[41] A. Denbleyker, Y. Liu, Y. Meurice, M. P. Qin, T. Xiang, Z. Y. Xie, J. F. Yu, and H. Zou, Phys. Rev. D **89**, 016008 (2014).
[42] J. F. Yu, Z. Y. Xie, Y. Meurice, Y. Liu, A. Denbleyker, H. Zou, M. P. Qin, J. Chen, and T. Xiang, Phys. Rev. E **89**, 013308 (2014).
[43] S. R. White, Phys. Rev. Lett. **69**, 2863 (1992).
[44] S. Östlund and S. Rommer, Phys. Rev. Lett. **75**, 3537 (1995).
[45] M. P. A. Fisher, P. B. Weichman, G. Grinstein, and D. S. Fisher, Phys. Rev. B **40**, 546 (1989).
[46] H. Zou *et al.*, Phys. Rev. A **90**, 063603 (2014).
[47] A. Bazavov, Y. Meurice, S.-W. Tsai, J. Unmuth-Yockey, and J. Zhang, Phys. Rev. D **92**, 076003 (2015).
[48] M. Fagotti and P. Calabrese, J. Stat. Mech. Theor. Exp. **2011**, P01017 (2011).
[49] P. Calabrese, M. Campostrini, F. Essler, and B. Nienhuis, Phys. Rev. Lett. **104**, 095701 (2010).
[50] P. Calabrese and F. H. L. Essler, J. Stat. Mech. Theor. Exp. **2010**, P08029 (2010).
[51] J. Unmuth-Yockey, J. Zhang, P. Preiss, L.-P. Yang, S.-W. Tsai, and Y. Meurice, Phys. Rev. A **96**, 023603 (2017).
[52] R. Islam, R. Ma, P. M. Preiss, M. E. Tai, A. Lukin, M. Rispoli, and M. Greiner, Nature (London) **528**, 77 (2015).
[53] A. J. Daley, H. Pichler, J. Schachenmayer, and P. Zoller, Phys. Rev. Lett. **109**, 020505 (2012).
[54] A. M. Kaufman, M. E. Tai, A. Lukin, M. Rispoli, R. Schittko, P. M. Preiss, and M. Greiner, Science **353**, 794 (2016).
[55] P. Preiss (private communication).
[56] L.-P. Yang, Y. Liu, H. Zou, Z. Y. Xie, and Y. Meurice, Phys. Rev. E **93**, 012138 (2016).
[57] P. Hasenfratz and F. Karsch, Phys. Lett. **125B**, 308 (1983).
[58] R. Savit, Rev. Mod. Phys. **52**, 453 (1980).
[59] D. Banerjee and S. Chandrasekharan, Phys. Rev. D **81**, 125007 (2010).
[60] T. D. Cohen, Phys. Rev. Lett. **91**, 222001 (2003).
[61] E. Fradkin and L. Susskind, Phys. Rev. D **17**, 2637 (1978).
[62] J. B. Kogut, R. B. Pearson, and J. Shigemitsu, Phys. Rev. Lett. **43**, 484 (1979).
[63] F. Lange, S. Ejima, and H. Fehske, Phys. Rev. B **92**, 041120 (2015).
[64] M. Dalmonte, E. Ercolessi, and L. Taddia, Phys. Rev. B **84**, 085110 (2011).
[65] Y. Zhang, T. Grover, and A. Vishwanath, Phys. Rev. Lett. **107**, 067202 (2011).
[66] Version 2.7.10, http://itensor.org/.
[67] J. Cardy and P. Calabrese, J. Stat. Mech. (2010) P04023.
[68] F. Verstraete, J. J. García-Ripoll, and J. I. Cirac, Phys. Rev. Lett. **93**, 207204 (2004).
[69] F. Verstraete, D. Porras, and J. I. Cirac, Phys. Rev. Lett. **93**, 227205 (2004).
[70] A. E. Feiguin and S. R. White, Phys. Rev. B **72**, 220401 (2005).
[71] M. Ogilvie and G. Guralnik, Nucl. Phys. **B190**, 325 (1981).
[72] M. Klomfass, U. M. Heller, and H. Flyvbjerg, Phys. Lett. B **258**, 386 (1991).
[73] F. Bruckmann, C. Gattringer, T. Kloiber, and T. Sulejmanpasic, Phys. Rev. D **94**, 114503 (2016).
[74] D. R. T. Jones, J. Kogut, and D. K. Sinclair, Phys. Rev. D **19**, 1882 (1979).